Acta Crystallographica Section D
Biological Crystallography
ISSN 0907-4449

Structural changes in a cryo-cooled protein crystal owing to radiation damage

Wilhelm Pascal Burmeister

European Synchrotron Radiation Facility, BP 220, F-38043 Grenoble CEDEX, France

Correspondence e-mail: wpb@esrf.fr

Received 8 October 1999
Accepted 7 January 2000

PDB References: data set 0, 1dwa; data set 1, 1dwf; data set 2, 1dwg; data set 3, 1dwh; data set 4, occupancy refinement, 1dwi; data set 4, positional refinement, 1dwj.

The high intensity of third-generation X-ray sources, along with the development of cryo-cooling of protein crystals at temperatures around 100 K, have made it possible to extend the diffraction limit of crystals and to reduce their size. However, even with cryo-cooled crystals, radiation damage becomes a limiting factor. So far, the radiation damage has manifested itself in the form of a loss of overall diffracted intensity and an increase in the temperature factor. The structure of a protein (myrosinase) after exposure to different doses of X-rays in the region of 20×10^{15} photons mm^{-2} has been studied. The changes in the structure owing to radiation damage were analysed using Fourier difference maps and occupancy refinement for the first time. Damage was obvious in the form of breakage of disulfide bonds, decarboxylation of aspartate and glutamate residues, a loss of hydroxyl groups from tyrosine and of the methylthio group of methionine. The susceptibility to radiation damage of individual groups of the same kind varies within the protein. The quality of the model resulting from structure determination might be compromised owing to the presence of radiolysis in the crystal after an excessive radiation dose. Radiation-induced structural changes may interfere with the interpretation of ligand-binding studies or MAD data. The experiments reported here suggest that there is an intrinsic limit to the amount of data which can be extracted from a sample of a given size.

1. Introduction

For a long time, radiation damage has been a major limiting factor in protein crystal data collection. When the cryocooling of crystals became available (Hope, 1988), this problem seemed to be overcome. The high X-ray flux of third-generation synchrotron sources now allows data collection on very small crystals or the collection of data sets to very high resolution. However, radiation damage is clearly becoming the limiting factor. This is aggravated in experiments using the multiple anomalous dispersion (MAD) technique, where several data sets have to be collected on the same crystal. Radiation damage in cryo-cooled protein crystals was first described by Gonzalez *et al.* (1992) and was studied further by Gonzalez & Nave (1994). At that time, damage was only observed with white-beam irradiation, as used for Laue experiments. The authors described the damage qualitatively as a loss of resolution of the diffraction pattern and an increase in the mosaicity of the crystal. In general, on a synchrotron beamline the damage is observed in the form of a reduction in the diffracted intensity and an increase in the temperature factor. To some extent, the scaling programs at the data-reduction step take care of this problem through a

variation of the scale factors and temperature factors throughout the data collection.

On the other hand, there is a vast literature about the effects of X-ray, γ-ray and electron irradiation of biomolecules such as peptides, amino acids and proteins. They have mainly been studied by electron-spin resonance and spectroscopic techniques. von Sonntag (1987) gives a good overview of this field. The primary effects of the X-ray irradiation of a protein crystal are the ejection of electrons from atoms through the photoelectric effect and through Compton scattering. The photons interact with the solvent as well as directly with the protein. Both components of the protein crystal have rather similar absorption cross sections. In the solvent, we particularly expect formation of hydroxyl radicals, as well as hydrated electrons, protons, hydrogen radicals and hydrogen gas (von Sonntag & Schuchmann, 1994). The hydroxyl radicals readily react with the protein by hydrogen abstraction, especially from N atoms of the backbone amides (Rao & Hayon, 1974). Other mechanisms include the capture of solvated electrons with or without subsequent protonation and the addition of atomic hydrogen and hydroxyl radicals. The question of the relative importance of these processes in the glassy environment of a protein crystal at 100 K remains open. In the presence of a high concentration of SO_4^{2-} ions, as in the case of myrosinase, a large amount of $SO_4^{2-\bullet}$ radical, which is a strong electron acceptor (von Sonntag & Schuchmann, 1994), should be formed within the solvent. In the protein itself, we should observe the formation of positively charged holes arising from the ejection of electrons and negatively charged radicals arising from the capture of free electrons. According to the results of Jones *et al.* (1987), at liquid-nitrogen temperature the electron-loss centres are trapped, forming amido radicals on the backbone after the loss of the proton. The captured electrons remain mobile until they reach an electrophilic centre.

Some of the most likely radical reactions are shown in Fig. 1. A disulfide bridge is a strong electrophilic centre where an ($RSSR^-$) radical is preferentially formed (1*a*). This radical was extensively described by Rao *et al.* (1983) and this reaction (1*a*) can occur efficiently for buried disulfide bridges. The disulfide bond of the ($RSSR^-$) radical can be cleaved spontaneously, as shown in (1*b*), or by protonation, as shown in (1*c*) (von Sonntag, 1987). Other studies on X-ray irradiation of single crystals of small compounds at 4.2 K (Box *et al.*, 1969) and of hydroxyl radical attack of aqueous solutions at room temperature (Bonifacic & Asmus, 1976) showed the formation of ($RSSR^+$) radicals as in reactions (1*d*) and (1*e*). In the ($RSSR^+$) radical, a cleavage of the disulfide bond can be initiated by hydroxyl ions (1*f*; Bonifacic *et al.*, 1975). A cleavage of the disulfide bond can be caused directly by the attack of hydroxyl radicals (1*g*; Bonifacic *et al.*, 1975).

Cysteine residues can lose their sulfhydryl group under attack by electrons or atomic hydrogen, leading to the formation of an alanyl radical and hydrogen sulfide (2*a*,*b*; von Sonntag, 1987). Another well established reaction is the trapping of holes by carboxylic acids (3*a*), which leads to a decarboxylation reaction (3*b*; Box *et al.*, 1969, 1972; Sevilla *et al.*, 1979). For tyrosine residues, the formation of a tyrosyl phenoxyl radical (4*a*,*b*) has been shown (Sevilla *et al.*, 1979). For methionine, the cleavage of a carbon–sulfur bond as shown in (5) has been observed, yielding α-amino-*n*-butyric acid and CH_3SH (Shimazu *et al.*, 1964). The detailed mechanism has not yet been established.

So far, the effects of irradiation of a cryo-cooled protein crystal on the protein structure have not been studied systematically. During experiments on the undulator beamline ID14-3 at the European Synchrotron Radiation Facility (ESRF), it became obvious that disulfide bonds were broken by the X-ray irradiation of protein crystals. Radiation damage, in the form of a reduction in diffraction and an increase in temperature factors, was also observed. These observations suggested that there might be further well defined structural changes upon X-ray exposure. The breakage of disulfide bridges in data sets collected with high X-ray doses from frozen crystals was probably first observed by Burmeister *et al.* (1994). However, at that time the reason for the absence of the disulfide bond was not known and was attributed to incomplete formation of the disulfide bonds in the cell or to reduction by reducing agents such as dithiothreitol present during purification. An opened disulfide bridge after a data collection using a high X-ray dose has also been reported by Berthet-Colominas *et al.* (1999). Weik *et al.* (2000) recently observed the opening of disulfide bridges owing to X-ray irradiation of acetylcholinesterase crystals.

Disulfide bridge

$$\text{(p)-CH}_2\text{SSCH}_2\text{-(p)} + e^- \longrightarrow \text{(p)-CH}_2\text{SS}^{\bullet -}\text{CH}_2\text{-(p)} \quad (1a)$$

$$\text{(p)-CH}_2\text{SS}^{\bullet -}\text{CH}_2\text{-(p)} \longrightarrow \text{(p)-CH}_2\text{S}^- + \text{(p)-CH}_2\text{S}^{\bullet} \quad (1b)$$

$$\text{(p)-CH}_2\text{SS}^{\bullet -}\text{CH}_2\text{-(p)} + H^+ \longrightarrow \text{(p)-CH}_2\text{SH} + \text{(p)-CH}_2\text{S}^{\bullet} \quad (1c)$$

$$\text{(p)-CH}_2\text{SSCH}_2\text{-(p)} \longrightarrow \text{(p)-CH}_2\text{SS}^{\bullet +}\text{CH}_2\text{-(p)} + e^- \quad (1d)$$

$$\text{(p)-CH}_2\text{SSCH}_2\text{-(p)} + \text{OH}^{\bullet} \longrightarrow \text{(p)-CH}_2\text{SS}^{\bullet +}\text{CH}_2\text{-(p)} + \text{OH}^- \quad (1e)$$

$$\text{(p)-CH}_2\text{SS}^{\bullet +}\text{CH}_2\text{-(p)} + \text{OH}^- \longrightarrow \text{(p)-CH}_2\text{SOH} + \text{(p)-CH}_2\text{S}^{\bullet} \quad (1f)$$

$$\text{(p)-CH}_2\text{SSCH}_2\text{-(p)} + \text{OH}^{\bullet} \longrightarrow \text{(p)-CH}_2\text{SOH} + \text{(p)-CH}_2\text{S}^{\bullet} \quad (1g)$$

Cysteine

$$\text{(p)-CH}_2\text{SH} + e^- \longrightarrow \text{(p)-CH}_2^{\bullet} + \text{SH}^- \quad (2a)$$

$$\text{(p)-CH}_2\text{SH} + \text{H}^{\bullet} \longrightarrow \text{(p)-CH}_2^{\bullet} + \text{H}_2\text{S} \quad (2b)$$

Aspartate and Glutamate

$$\text{(p)-CH}_2\text{CH}_2\text{COO}^- \longrightarrow \text{(p)-CH}_2\text{C}^{\bullet +}\text{H}_2\text{'COO}^- + e^- \quad (3a)$$

$$\text{(p)-CH}_2\text{C}^{\bullet +}\text{H}_2\text{COO}^- \longrightarrow \text{(p)-CH}_2\text{CH}_2^{\bullet} + \text{CO}_2 \quad (3b)$$

Tyrosine

$$\text{(p)-CH}_2\text{C}_6\text{H}_4\text{OH} \longrightarrow \text{(p)-CH}_2\text{C}_6\text{H}_4\text{OH}^{\bullet +} + e^- \quad (4a)$$

$$\text{(p)-CH}_2\text{C}_6\text{H}_4\text{OH}^{\bullet +} \longrightarrow \text{(p)-CH}_2\text{C}_6\text{H}_4\text{O}^{\bullet} + H^+ \quad (4b)$$

Methionine

$$\text{(p)-CH}_2\text{CH}_2\text{SCH}_3 + 2\text{H}^{\bullet} \longrightarrow \text{(p)-CH}_2\text{CH}_3 + \text{CH}_3\text{SH} \quad (5)$$

Figure 1
Radical reactions caused by X-ray or electron irradiation which are likely to contribute to the observed radiation damage to the amino-acid side chains. (p)- represents protein. References for the reactions are given in the text. The mechanism for reaction (5) is not known; only the products have been identified (Schimazu *et al.*, 1964).

This study addresses the effect of an increasing radiation dose on the structure of a protein in a cryo-cooled crystal. The radiation doses which were studied were chosen in the region of 20×10^{15} photons mm^{-2}, which is typical of a data collection at a third-generation synchrotron source. A relatively large protein, myrosinase, a glycosidase of 65 kDa, was used as a test case. The crystals diffract to high resolution (1.2 Å) and the protein contains disulfide bridges and a bound zinc ion; it is extensively glycosylated. Compared with crystals of smaller proteins such as hen egg-white lysozyme, which are very often used as test samples for diffraction experiments, myrosinase has more residues in a variety of environments. Furthermore, the effect of radiation damage on glycosylation and metal sites can be studied.

A loss of electron density for certain types of groups has been shown from this work. These comprise S atoms of disulfide bridges and cysteines, as well as carboxyl groups of glutamic and aspartic acid residues, hydroxyl groups of tyrosine residues and methylthio groups of methionine. This loss of electron density can be explained by chemical modifications of residues owing to radiation-induced reactions which occur in the cryo-cooled crystal.

2. Methods

2.1. The crystal

Myrosinase crystals were prepared as described (Burmeister *et al.*, 1997) by the hanging-drop method using 66% saturated ammonium sulfate, 100 m*M* HEPES pH 6.5 as precipitant. For cryoprotection, a crystal was transferred to a solution containing 66%(*v*/*v*) saturated ammonium sulfate solution, 100 m*M* HEPES pH 6.5 and 10%(*v*/*v*) glycerol and kept there for a few minutes. Before it was frozen directly in the nitrogen stream it was dipped for a few seconds into an equivalent solution containing 20% glycerol.

2.2. Irradiation and flux measurements

The study was carried out on the experimental station ID14-3 at the ESRF at a wavelength of 0.9475 Å (13.08 keV). The optical system of the beamline, consisting of a diamond (111) and a germanium (220) monochromator crystal and a multilayer mirror (Burmeister *et al.*, 1998), leads to an X-ray beam without detectable harmonic contamination. For the study, the standard setup at the experimental station was used. The beam size at the sample was 0.15 × 0.15 mm, defined by the slits of the collimating system. The beam was slightly defocused vertically in order to obtain an uniform illumination of the sample. The crystal with a diameter of 0.1 mm and a length of 0.3 mm was oriented along the spindle axis. During the exposure time the crystal was rotated slowly in order to obtain an uniform exposure.

The flux was measured using a windowless silicon PIN photodiode from Hamamatsu, type S3590-04. It was protected against ambient light with 25 µm of black Kapton foil (Goodfellow). The thickness of the diode was 0.3 mm and its size was 10 × 10 mm. The diode was operated using a reverse voltage of 70 V. The flux was determined using an absorption of 65% of 0.3 mm thick silicon at 13.08 keV (calculated with the program *XOP*; Dejus & Sanchez del Rio, 1996) and a yield of 0.26 ± 0.01 A W^{-1} absorbed power. This value was taken from the documentation of IRD, Torrance, USA, and from Rabus *et al.* (1996). The final conversion factor was 2.7×10^{9} photons s^{-1} µA^{-1}. This measurement of the flux was used in order to calibrate the ion chamber (using air as the active medium), which was located between the collimating slits and the sample. The linearity of the response of the diode and the ion chamber was verified using up to six 0.25 mm thick aluminium foils (Goodfellow) as attenuators. The absolute error of the flux measurements was estimated to be about 10%.

Using *XOP*, the linear absorption coefficient for the photoelectric effect was calculated to be about 0.43 mm^{-1} for the myrosinase crystal with a composition of about 50% solvent (2.7 *M* ammonium sulfate) and 50% protein. Considering the sample as small compared with the absorption length, this gave a dose of 0.43 photons mm^{-3} absorbed in the sample for a dose of 1 photon mm^{-2}. This corresponds to an absorbed dose of 5.6 keV mm^{-3} or, using the calculated density of the crystal of 1.25 g cm^{-3}, to a dose of 7.2×10^{-10} Gy (J kg^{-1}). Throughout the experiment the unit of photons mm^{-2} was used, as the other units depend on the exact composition and density of the crystal.

2.3. Cooling and data collection

An Oxford Cryosystems cooling device was used in order to cool the crystal to 100 K (reading of the instrument) in a nitrogen-gas flow. The temperature of the crystal was verified using a K-type thermocouple made from 25 µm diameter wires, which was placed coaxially in the flow. At the position of the crystal the thermocouple showed a temperature below 110 K.

Diffraction data were collected using a MAR CCD area detector with a 133 mm diameter. The crystal-to-detector distance was 118.0 mm. Five data sets were collected using the same angular range as well as approximately the same radiation dose per exposure. Each data set consisted of 92 images with a 1° oscillation angle collected with three passes per exposure. The exposure time for the different data sets varied between data sets from 2.04 to 2.46 s per image depending on the flux at the sample position, which was between 2.0 and 2.5×10^{12} photons mm^{-2} s^{-1}. Data sets were processed with *MOSFLM* (Leslie, 1990) and *CCP*4 software (Collaborative Computational Project, Number 4, 1994), using similar command files and the same orientation matrix and unit-cell parameters. The statistics of the data sets are shown in Table 1. The X-ray dose for the collection of each data set was 0.15×10^{15} photons mm^{-2}. The first data set is data set 0. Because it should truly represent the state before irradiation, the lowest possible dose has been used for its collection, thereby limiting the maximal resolution. Between the data sets, the crystal was exposed to a dose of 8.9×10^{15} photons mm^{-2} (data sets 1, 2 and 3) and to 26.7

$\times 10^{15}$ photons mm^{-2} before the last data set (data set 4); see also Fig. 2(*b*).

2.4. Difference map calculation

Difference maps were calculated using σ_A-weighted phases derived from the 1.2 Å resolution myrosinase model (Burmeister *et al.*, 2000). A rigid-body and overall anisotropic *B*-factor refinement using *REFMAC* (Murshudov *et al.*, 1999) against data set 0 has been carried out in order to take into account overall temperature-factor changes and to obtain σ_A weights. The r.m.s. value of the positional shifts of the atoms owing to the rigid-body refinement was 0.1 Å and may be a consequence of a small anisomorphism of individual crystals. The structure-factor amplitudes of data sets 1 to 4 were scaled using *SCALEIT*. Difference Fourier maps were calculated to 2.4 Å resolution on an approximate absolute scale using the unit-cell parameters of the reference data set.

2.5. Occupancy refinement

The 1.2 Å structure with isotropic temperature factors was used as the starting model. First, the temperature factors of the structure were refined against data set 0 using *X-PLOR* (Brünger, 1992*a*). This step was included in order to reduce bias in the temperature factors from the high-resolution structure, which showed some signs of radiation damage. The resulting model has been used for all other occupancy refinements carried at 2.0 Å resolution. No further refinements of individual atomic temperature factors have been carried out, as they are strongly correlated with the occupancies. $R_{\rm free}$ (Brünger, 1992*b*) was calculated based on 2558 (5%) reflections. The changes in the unit-cell dimensions have not been taken into account. This treatment is justified if an uniform and isotropic expansion of the unit-cell contents (solvent and protein) is assumed.

The atoms of each type of group which was studied were grouped together and the overall occupancy of each group was refined using *X-PLOR*. These groups were (number of occurrences in brackets): S$^{\gamma}$ of cysteines in disulfide bridges (6); S$^{\gamma}$ of free cysteines (2); carboxyl groups of aspartic acid (37); carboxyl groups of glutamic acid (18); methylthio groups of methionine (8); hydroxyl groups of tyrosine (38); formamido groups of asparagine (37); formamido groups of glutamine (27); C$^{\beta}$, C$^{\gamma1}$ and C$^{\gamma2}$ of valine (20); C$^{\gamma}$, C$^{\delta1}$ and C$^{\delta2}$ of leucine (36); C$^{\beta}$ of aspartic acid (37); C$^{\beta}$ and C$^{\gamma}$ of glutamic acid (18). The occupancies of the groups were refined simultaneously while all temperature factors remained fixed. The same protocol was used for the refinement against each of the five data sets. The statistics of the refinements are given in Table 1.

A second occupancy refinement was performed using individual groups. Only groups with atoms which had small temperature factors (<35 Å^2) and which had no alternate conformations in the 1.2 Å structure were used. Prior to occupancy refinement, the overall temperature factor of the structure was refined and the occupancies of these groups were assigned random values between 0 and 1. Temperature factors remained fixed during this refinement. The occupancy was refined until convergence. Statistics are shown in Table 1. Using an additional rigid-body refinement of the protein structure prior to occupancy refinement had no significant effect on the resulting occupancies (results not shown).

2.6. Positional refinement

Positional refinement was performed for data set 4 using as a starting model the results of the individual group occupancy refinement for that data set. It was assumed that the loss of disulfide bridges in the crystal was complete for this data set and consequently the disulfide bridges were removed from the topology file. The occupancy of the S$^{\gamma}$ atoms was reset to unity. A random coordinate displacement with a maximum ampli-

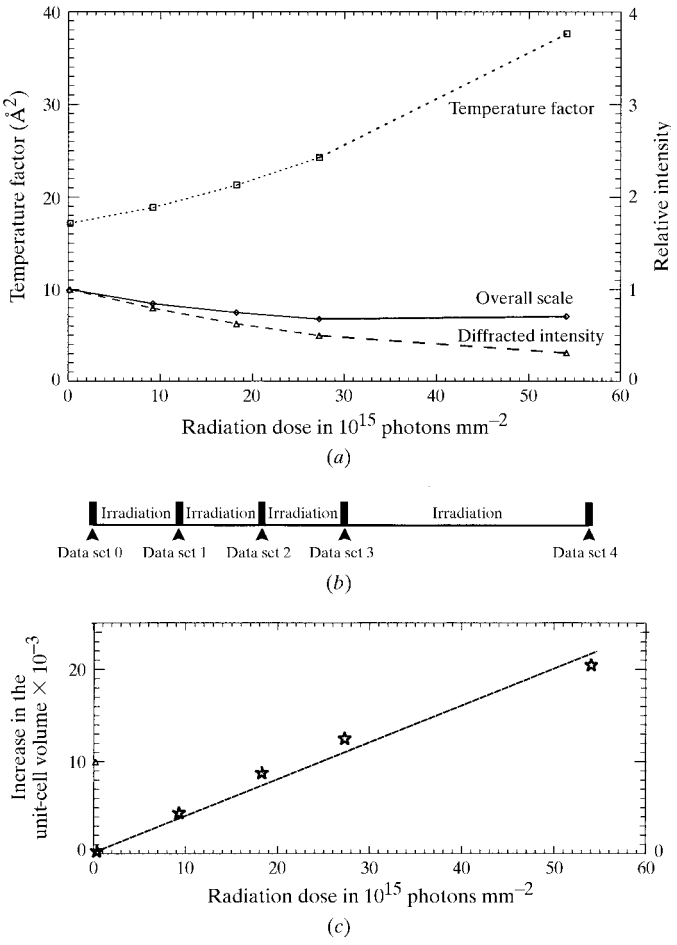

Figure 2
Global changes in the diffraction data as a function of the radiation dose. (*a*) The total intensity of the measured reflections normalized to 1 for data set 0 (triangles), the overall scale factor compared with the first data set (rhombi) and the overall temperature factor (squares) are plotted as a function of the radiation dose. The total intensity is the sum of all *I*s written into the MTZ file after integration by *MOSFLM* corrected for the incident flux. The scale factors and temperature factors have been calculated with *TRUNCATE*. (*b*) Experimental scheme. Short data collections alternate with long irradiations of the crystal. The dose used for the collection of a data set is small compared with the dose deposited during the irradiations. (*c*) The relative change in the unit-cell volume is plotted *versus* the radiation dose. The unit cell has been refined by *MOSFLM* during the integration.

Table 1
Statistics of the data sets (R_{merge}) and the refinement.

The five data sets were collected using the same angular range, the same dose per data set and the same parameters for the integration. The completeness is 99.8 (99.8)%, the redundancy 3.4 (3.0), about 250 reflections were rejected as bad spots by *MOSFLM* and less than eight reflections per data set were overloads. Values given in parentheses refer to the highest resolution bin (2.00–2.07 Å). The crystallographic *R* factors with the starting model involving only anisotropic temperature-factor refinement are given. The R_{free} and R_{work} values after the two refinement protocols (refinement of one occupancy per type of group and the refinement of occupancies of each individual group) are also listed.

Set	Dose (10^{15} e$^-$ mm^{-2})	R_{merge} (%)			R_{free} after overall *B*-factor refinement (%)	R_{work} after overall *B*-factor refinement (%)	R_{free} after grouped occupancy refinement (%)	R_{work} after grouped occupancy refinement (%)	R_{free} after individual occupancy refinement (%)	R_{work} after individual occupancy refinement (%)
		Total	2.6–2.4 Å	2.1–2.0 Å						
0	0.1	4.6	5.4	14.2	17.7 (21.9)	16.4 (20.6)	17.8 (22.1)	16.4 (20.6)	17.9 (23.5)	16.5 (22.0)
1	9.1	4.9	6.0	14.7	17.9 (22.7)	17.0 (22.4)	17.9 (23.0)	16.8 (22.4)	18.0 (24.5)	16.9 (23.6)
2	18.2	5.1	7.0	18.6	19.4 (25.9)	18.7 (25.1)	19.3 (24.8)	18.4 (26.1)	19.3 (27.2)	18.4 (25.8)
3	27.2	5.6	9.0	25.9	21.8 (31.7)	21.0 (48.9)	21.6 (31.3)	20.5 (28.1)	21.7 (32.5)	20.5 (29.0)
4	54.0	8.1	26.1	95.8	28.9 (52.4)	28.7 (50.4)	28.5 (52.6)	28.0 (50.0)	28.6 (53.0)	28.0 (51.2)

tude of 0.2 Å in each coordinate was added to the atom positions in order to reduce bias prior to positional refinement using a standard crystallographic energy-minimization protocol at 2.4 Å resolution. As negative difference electron density remained at the new position of the S atoms, the individual occupancy of these atoms was refined. For verification, an analogous protocol was used with data set 0 (including the constraints for disulfide bridges). R_{work} after refinement was 18.6% and R_{free} was 24.5% for data set 4. For data set 0, these values were 15.3 and 18.7%, respectively.

2.7. Structure analysis

The environment of the groups prone to radiation damage was analysed using computer graphics (*O*; Jones *et al.*, 1993) and by a calculation of the solvent accessibility using *X-PLOR* and a probe radius of 1.35 Å.

3. Results

3.1. Overall damage

The most obvious sign of radiation damage in the myrosinase crystal is a dramatic decrease in the total diffracted intensity (Fig. 2). This loss can be fitted with an exponential function $\exp(-d/D)$ with a constant D of 42×10^{15} photons mm^{-2}. This decay arises from a dramatic increase in the temperature factor, whereas there is only a moderate decrease of the scale factor when the data are brought onto an absolute scale. This scale factor is proportional to the fraction of atoms in the crystal contributing to the coherent diffraction. A reduction could mean a loss of mass of the protein owing to radiolysis.

A more subtle but still very interesting effect is the change in the unit-cell volume (Fig. 1*c*). This effect is described for a number of proteins by Ravelli & McSweeney (2000). In contrast to the other effects, which show an exponential decay, this effect seems to be linear with the dose. In the refinements against data set 4 described in §§2.5 and 2.6, three models of unit-cell expansion have been tried: assumption of a uniform expansion of protein and solvent, a uniform expansion combined with a rigid-body movement of the protein, and the protein moving as a rigid body but keeping its size. As the structure factors depend only on the fractional coordinates, an uniform expansion of unit-cell parameters and protein model is equivalent to the use of the original unit cell and coordinates in the refinement. As the use of the real unit cell combined with rigid-body refinement strongly degraded the *R* factors and the rigid-body refinement using the original unit cell hardly improved the *R* factors, it was assumed that the model of a uniform expansion of the protein crystal is most realistic. Thus, the unit cell and atom positions of the first data set can be used throughout the study. It cannot be completely ruled out that the apparent increase of the unit-cell size arises from an artefact of the refinement and indexing programs, as the intensity and effective resolution of the images used in auto-indexing and parameter refinement decreases through the different data sets.

3.2. Structural changes arising from radiation damage

A comparison of the structure of the crystal before and after irradiation by means of difference Fourier maps shows peaks which are clearly located on certain types of groups. The most obvious effect is the appearance of negative electron-density peaks at the position of the disulfide bridges (Fig. 3*a*) accompanied by some positive electron-density peaks in proximity. These can be explained (see below) by an opening of the disulfide bridge accompanied by an additional loss of electron density for the S atoms.

Other negative electron-density peaks (corresponding to a loss of electron density after irradiation) occur at the position of carboxyl groups of aspartic acid groups (Fig. 3*b*) and glutamic acid groups (Fig. 3*c*) as well as on the methylthio groups of methionine (Fig. 3*d*) and at the position of the hydroxyl groups of some of the tyrosine residues (Fig. 3*c*). The strong negative electron density for the carboxylic acids was particularly striking, as it did not occur on the otherwise closely related residues asparagine and glutamine. Exceptions are the active-site residue Gln187 and Asn466 shown in Fig. 3(*b*), which will be discussed later. Positive electron-density peaks are less significant and are always near negative electron-density peaks.

Table 2
Rate constants obtained for different labile groups.

The average rate constants were obtained by an exponential fit $q = \exp(-d/D)$, where q is the occupancy, d is the dose and D is a rate constant, to the results from the occupancy refinement where all groups of the same kind were refined together. The fastest rate obtained from the occupancy refinement of individual groups is also given. In the case of the disulfide bridge, a function of the form $q = (1 - a) \times \exp(-d/D) + a$ has been fitted and the fraction of the remaining occupancy a is given which arises from an overlap between the new and old positions of the S atoms after the breakage of the disulfide bridge.

	Average rate constant D for the labile group (10^{15} photons mm^{-2})	Smallest rate constant D for the labile group (10^{15} photons mm^{-2}); name of the residue
Breakage of disulfide bridge	17; 44% of occupancy remaining	16; 13% of occupancy remaining; Cys214
Carboxyl group of glutamate	110	50; Glu446
Carboxyl group of aspartate	130	70; Asp87
Methylthio group of methionine	160	90; Met393
Hydroxyl group of tyrosine	440	30; Tyr330

In order to obtain a quantitative estimate for the loss of electron density for certain groups, an occupancy refinement of the relevant groups was carried out. In order to avoid overfitting of the data, the minimum number of degrees of freedom were introduced. Thus, it was first assumed that all groups of the same kind are evenly susceptible to radiation damage and individual temperature factors were fixed. As a control, similar groups were chosen from residues presenting no obvious changes. In order to minimize bias, no positional refinement was carried out. This means that the results of the occupancy refinement (Fig. 4) can be interpreted in terms of a radiolysis of the group, of a disorder with several alternate positions or as a shift of the position of the group. The third case occurs in particular for the cysteine S^{γ} atoms, which both move when the disulfide bridge has been opened.

Essentially no reduction of electron density was observed for the controls (Fig. 4*d*), which were the side chain of valine, the terminal part of leucine and the formamido groups of asparagine and glutamine. This proves that the decreasing occupancy of the labile groups after the refinement is not an artefact of diminishing data quality or some other global effect because the controls are very similar to carboxyl groups. Interestingly, the aliphatic groups (Figs. 4*b*,*d*) refined to a higher occupancy than unity. This is a consequence of the considerable number of H atoms which are not taken into account in the structure-factor calculations (seven electrons from H atoms compared with 18 electrons from the C atoms in the case of a valine side chain). For aliphatic groups, the ratio of H atoms to scattering atoms is higher than average for a protein and thus the scattering of these groups is underestimated in a structure-factor calculation. An occupancy refinement will compensate for this by an increase of the occupancy beyond 1.0. The slight reduction of the occupancy of glutamine is probably largely because of a loss of electron density for Gln187, which will be discussed later.

From the difference Fourier maps it was obvious that the loss of electron density did not affect all chemically equivalent groups equally. In order to establish the difference in sensitivity, the next step was to refine the occupancies of the groups individually. All the groups show an almost monotonic decrease of the occupancy with increasing X-ray dose (Fig. 5), which can be fitted with an exponential decay. This is a verification of the result, as the refinements against the different data sets were carried out independently using different starting occupancies. The standard deviation of the difference of the refined occupancy and the fitted occupancy from the exponential curve is 0.022 for glutamate, 0.019 for aspartate, 0.015 for methionine and 0.034 for tyrosine, giving an estimation of the accuracy of the refinement. As expected, the occupancy refinement becomes more reliable with an increasing number of electrons in the group.

3.3. Disulfide bridges

The occupancies for the S^{γ} of the two free cysteines and for those in the three disulfide bridges are compared in Fig. 4(*a*). The disulfide bridges show an apparent loss in occupancy with a rate constant of 17×10^{15} photons mm^{-2} (Table 2). The loss of electron density of the disulfide bridges could arise from a movement of atoms, increasing disorder after opening of the bridge or from loss of the S atom. The free cysteines, on the other hand, seem to be much more stable and the decrease in electron density is less significant.

The refinement of individual occupancies showed a similar rate for the breakage of the three cysteine bridges of the protein (Fig. 5*a*). All these cysteines have a rather similar environment where they are partially exposed to solvent, allowing the access of a solvent probe to the C^{β} atom or to the S^{γ} atom. Cys438 is an exception, since it is almost fully exposed to solvent, with four water molecules within van der Waals distance. Out of the free cysteine residues, Cys73 appears to be quite labile (Fig. 5*a*), whereas the other one (Cys171) is completely stable. This is possibly related to the solvent accessibility, as Cys171 is fully buried inside the protein (C^{β} and S^{γ} atoms not accessible), whereas Cys73 is partially exposed to solvent, with two water molecules within a distance of 3.9 Å. After positional refinement of the structure against data set 4 it became obvious that the loss of occupancy in the disulfide bridges is only partially a consequence of a movement of the S^{γ} atoms; it is also attributable to a loss of the S^{γ} atoms. These occupancies are between 0.6 and 0.8 after positional and occupancy refinement against data set 4.

3.4. Carboxylic acid residues

The rate constants for the loss of electron density obtained for glutamate and aspartate groups (Fig. 4*b*) are similar (110×10^{15} and 130×10^{15} photons mm^{-2}, respectively; Table 2). A refinement of the aliphatic part of the groups shows a

much slower loss of electron density for glutamic acid and stable electron density for C^{β} of aspartate. This shows that only the carboxyl group is affected by the loss of electron density, which must be because of decarboxylation. The loss of density or order at the carboxyl position will lead to increased disorder at the glutamic acid C^{γ} position causing a small reduction of the total electron density for C^{β} and C^{γ}, as observed.

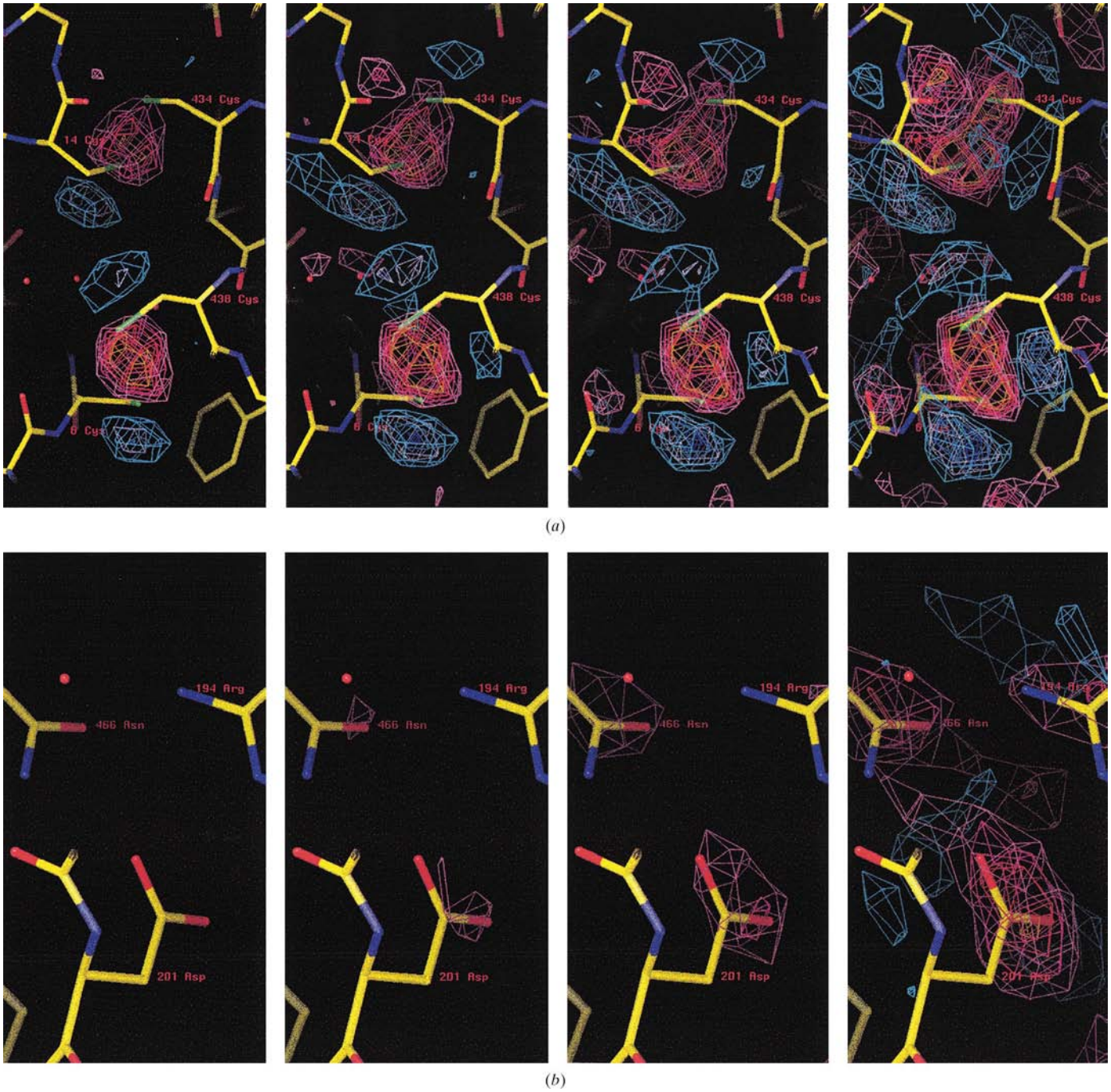

Figure 3
Difference Fourier electron-density maps showing the loss of electron density of side chains which are affected by radiation damage. The maps were calculated at 2.4 Å resolution using structure-factor amplitudes from the data sets 1 to 4 and model phases as described in §2. The reference structure-factor amplitudes are taken from data set 0 collected before irradiation. The contour levels are −0.25 (orange), −0.2 (red), −0.15 (pink), −0.1 (magenta), 0.1 (cyan), 0.15 (light blue), 0.2 (turquoise) and 0.25 e^{-} Å^{-3} (blue). The approximate absolute scale from *TRUNCATE* is used. The standard deviations of the electron-density maps are 0.013, 0.021, 0.028 and 0.056 e^{-} Å^{-3} for maps 1 to 4 (left to right), respectively. Doses for maps 1 to 4 (left to right) were 9×10^{15}, 18×10^{15}, 27×10^{15} and 54×10^{15} photons mm^{-2}, repectively. (*a*) Two of the disulfide bridges (Cys14–Cys434, Cys6–Cys438) of the protein. The positive densities next to the S atoms arise from movement of the S atoms. Positive density below residue 14 is a consequence of a relaxation of the main chain upon opening of the cysteine bridge. (*b*) Asp201. The loss of electron density of the aspartic acid residue is clear. A loss of order of the terminal part of Asn466 and Arg194 becomes visible for higher X-ray doses, owing to the loss of hydrogen bonds and salt bridges to Asp201.

The glutamic acid residues are reactive to a different extent (Fig. 5*b*). Most of them are well exposed to solvent. Only the carboxyl groups of Glu41 and Glu222 are more stable. The carboxyl group of Glu41 shows a very low exposure to solvent (2.6 Å^2). The solvent exposure of Glu222 is also quite low (12.2 Å^2) compared with an average solvent-accessible surface of about 30 Å^2 for the carboxyl groups. Another common feature of these two groups are salt bridges to arginine residues. On the other hand, salt bridges to arginine residues and relatively low solvent accessibility also occur for labile residues. Unfortunately, there are not enough glutamic acid residues in the protein to establish a significant correlation between radiation damage and the environment of the carboxyl group.

Aspartic acid residues again show a broad distribution in their reactivity towards decarboxylation. The solvent accessi-

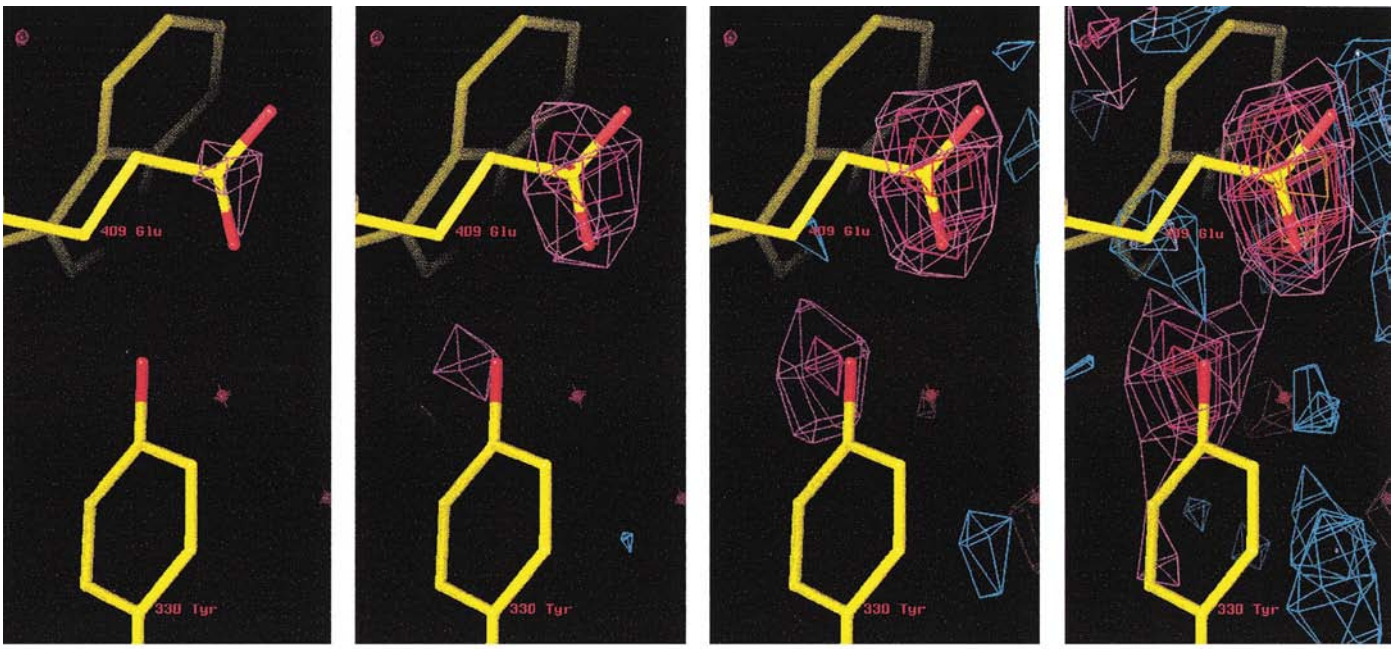

(*c*)

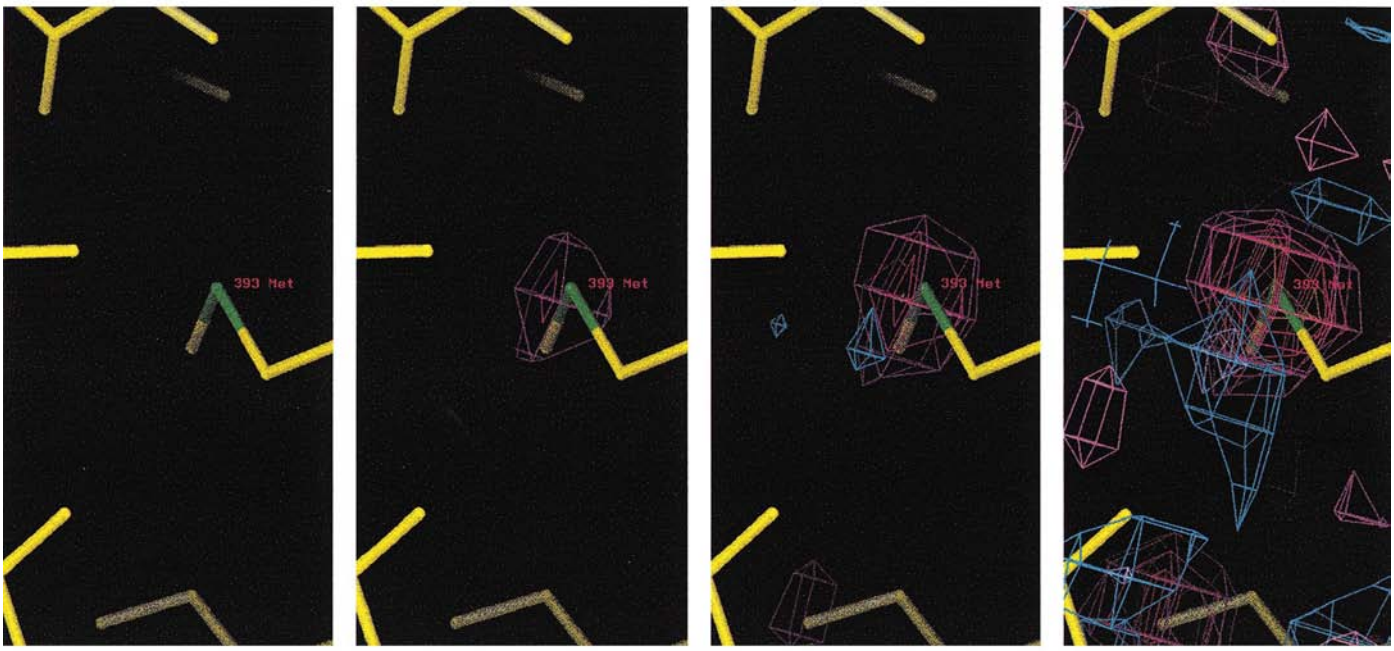

(*d*)

Figure 3 (continued)
(*c*) Glu409 and Tyr330 of the active site. These two amino acids form a very labile pair. At high doses, positive electron-density peaks appear in the solvent, indicating a change in the solvent structure owing to the loss of the carboxyl and hydroxyl groups. (*d*) Met393, one of the most labile methionine residues of the structure.

bility is widely scattered; some of these residues are fully buried inside the protein, although most are located on the surface. It is not possible to establish a correlation between the susceptibility towards decarboxylation and the degree of solvent accessibility of the carboxyl groups. The only residue with a completely different reactivity is Asp70, which provides its carboxyl group as a ligand to the structural Zn atom located on the twofold axis of the myrosinase dimer. This completely removes the sensitivity towards decarboxylation.

3.5. Tyrosine

Tyrosine residues show a strong variation in the stability of the hydroxyl group (Fig. 5*e*), which ranges from almost completely stable to very labile (Tyr330). Again, there is no significant difference in solvent accessibility between labile or stable residues. The presence of a hydrogen bond with a glutamic acid group and the lability of the hydroxyl group may be correlated. The three most labile hydroxyl groups form this type of salt bridge, especially the active-site residue Tyr330, which is the least stable tyrosine of the structure.

3.6. Methionine

A significant loss of electron density is observed for methylthio groups of methionine (Fig. 4*c*). Methionine residues show some variability in their sensitivity towards loss of the methylthio group (Fig. 5*d*). Interestingly, the most labile groups are either fully buried (Met393) and or have only a small accessible surface (0.7 Å^2) for their methylthio group (Met256).

3.7. Structural rearrangements

The refined model of the structure of the protein after an exposure to 54×10^{15} photons mm^{-2} shows a relaxation of the protein in proximity to lost disulfide bridges and in proximity

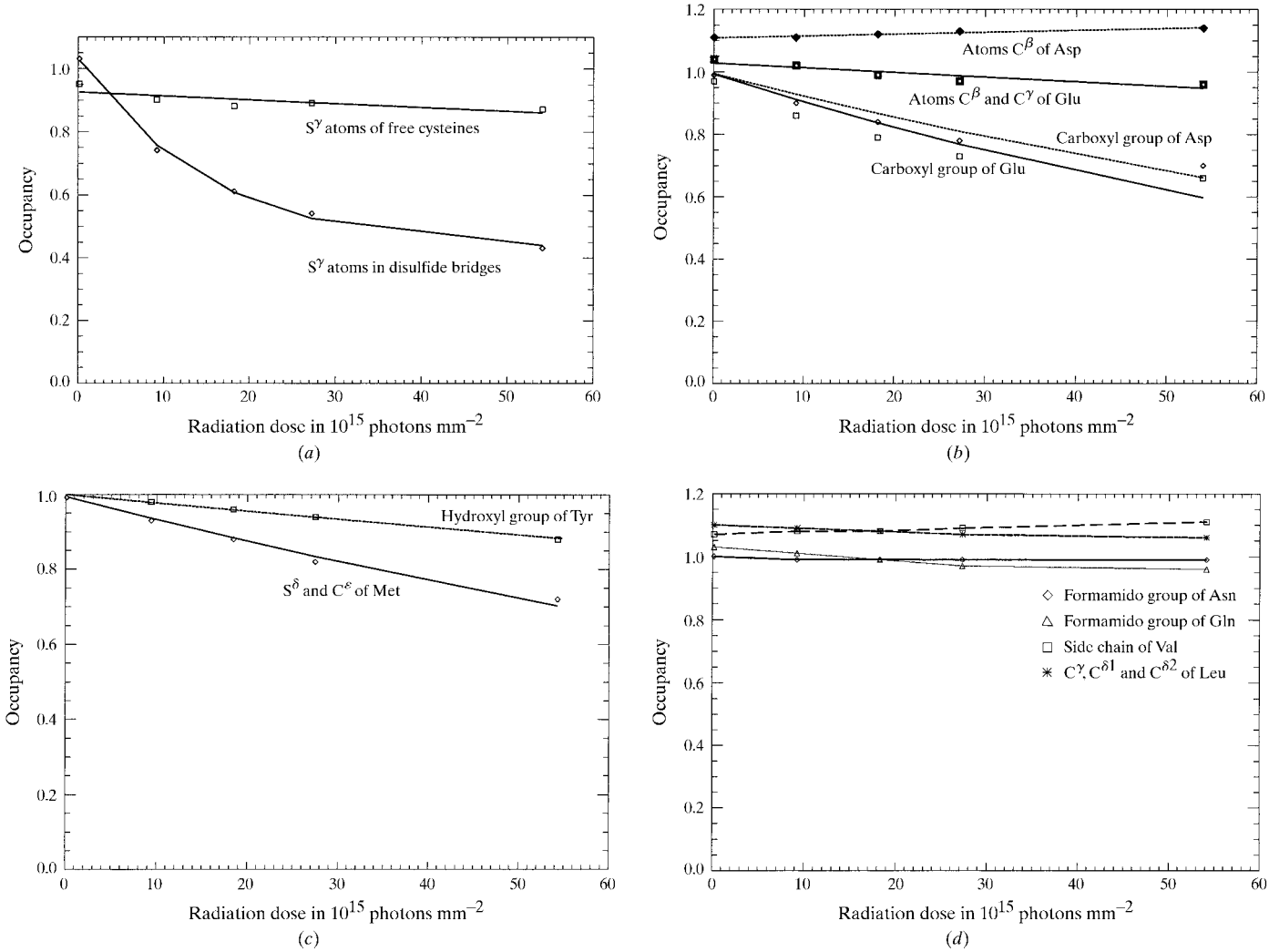

Figure 4
Refinement of occupancies of groups prone to radiation damage. The occupancy of all atoms belonging to groups of the same kind was refined together. An exponential decay of the occupancy with time constants given in Table 2 has been fitted. (*a*) Cysteines. The function fitted to the loss of occupancy of the disulfide bridges is $[(1 - a) \times \exp(-d/D) + a]$. This takes into account that the occupancy does not drop to zero upon opening of the disulfide bridge, as the new S^{γ} positions overlap with the old positions. It was assumed that the loss of S^{γ} in free cysteine residues is slow compared with the opening of the disulfide bridge. (*b*) Carboxylic acids. (*c*) Methionine and tyrosine. (*d*) Control experiments with stable groups. Linear regressions have been plotted.

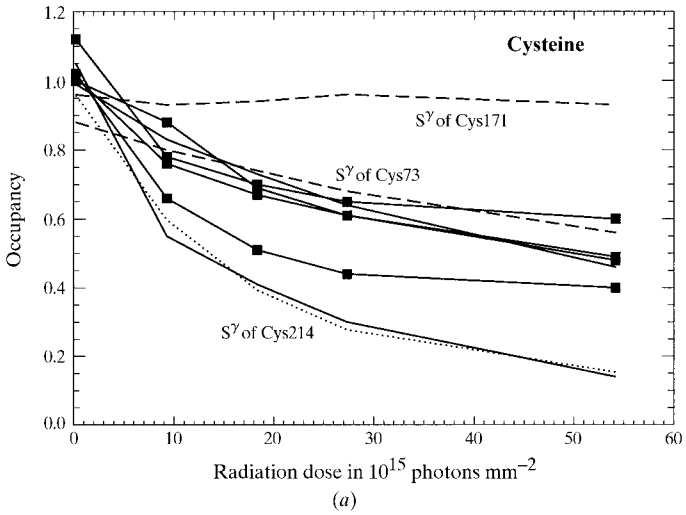

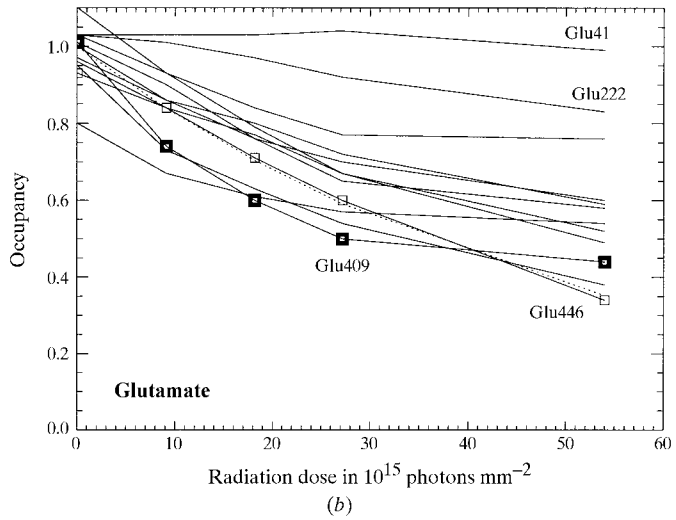

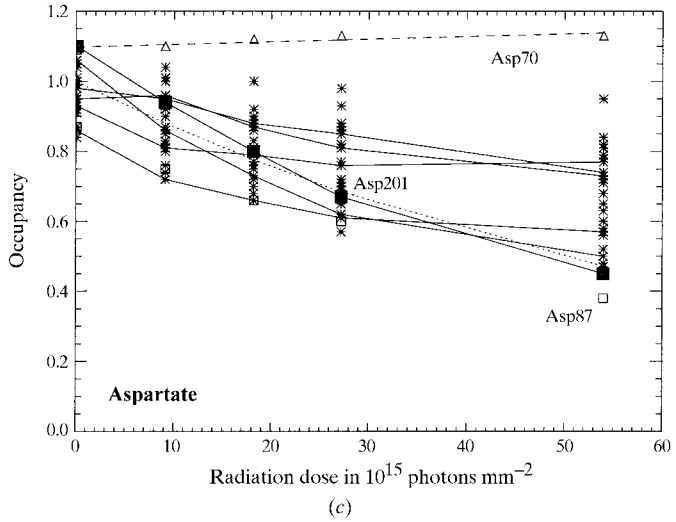

to other residues which showed a large loss in electron density. The changes in the region of the two disulfide bridges are shown in Fig. 6. There is good agreement between the reference structure and the structure refined against the data set taken before irradiation. This shows that the structural changes which occurred after irradiation are not a consequence of the refinement at lower resolution but arise because of irradiation. It is possible to explain the changes in the electron density by a movements of the protein chain together with a reduced occupancy for the S atoms of the cysteine residues. The weak residual electron density could be explained by the presence of other rotamers and part of the lost electron density for S^{γ} could arise from the presence of other rotamers which have not been modelled. There is no hint of oxidation of S atoms to form sulfonyl groups, but they could be ordered too poorly to be observed.

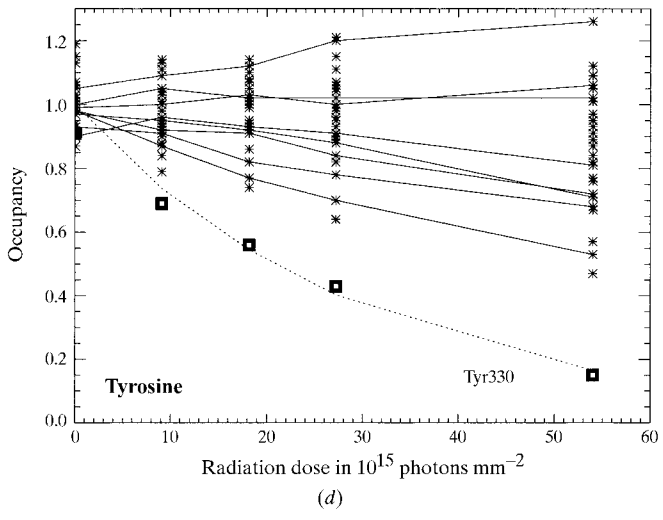

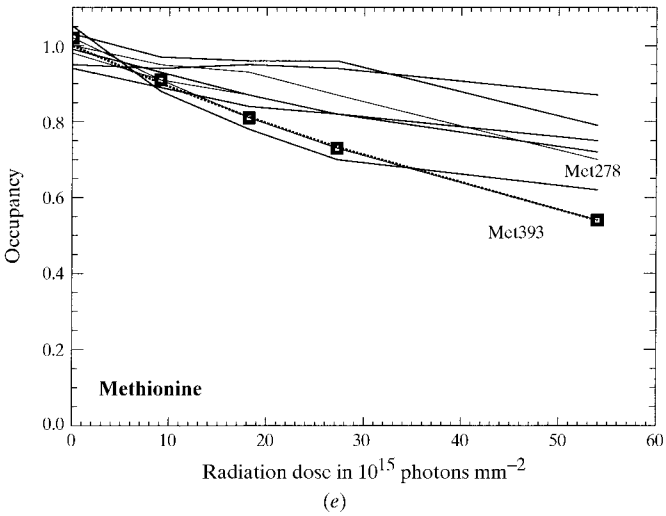

Figure 5
Individually refined occupancies of labile groups. The most rapid loss of electron density (plotted with squares, residue name given) is fitted with an exponential function (dotted line). The rate constants obtained from these fits are given in Table 2; the scatter of the points gives an idea of the statistical errors of the refined occupancies. The groups shown in Fig. 3 are plotted as black squares. (*a*) S atoms of free cysteines (dashed lines) and disulfide bridges (solid lines). (*b*) Carboxyl groups of glutamic acid residues. (*c*) Carboxyl groups of aspartate residues. For clarity, the connecting lines are only drawn for every fifth residue. Asp70 (triangles) is involved in the coordination of the Zn atom. (*d*) Hydroxyl groups of tyrosine. For clarity, the connecting lines are only drawn for every fifth residue. (*e*) Methylthio groups of methionine.

The movements in proximity of groups with a strong loss of electron density especially affect the active site of the protein. It seems that the loss of the carboxyl group of Glu409 leads to a disruption of the hydrogen-bond network in the active site, particularly affecting the residues Asn186, Gln187 and Arg95, which shift and become less ordered. For these residues there are significant negative peaks in the difference maps, even though these types of residues are stable everywhere else in the protein. In most parts of the protein, especially in the hydrophobic core, there are no significant shifts of the atom positions compared with the structure prior to irradiation.

4. Discussion

4.1. Overall radiation damage

The first global effect is an increase in the unit-cell size which is proportional to the radiation dose. This could arise from an expansion of the solvent part of the protein crystal, from an expansion of the protein, or both. A reason for the expansion of the solvent could be the loss of hydrogen bonds owing to the transformation of water molecules into radical species such as the hydroxyl radical. Gases like H_2 and CO_2 may accumulate in interstitial spaces.

The dose of about 42×10^{15} photons mm^{-2}, which reduces the diffracted intensity to $1/e$, can be converted into a dose of 3.1×10^7 Gy. Owing to the high concentration of ammonium sulfate in the solvent of the myrosinase crystal, the dose absorbed per flux is about a factor of two higher than for protein crystals grown under low-salt conditions.

The above dose of 3.1×10^7 Gy agrees very well with the dose of 2×10^7 Gy which Henderson (1990) postulated will destroy crystalline diffraction from a sample. Furthermore, there is also good agreement with the values from Gonzalez & Nave (1994), who observed extensive damage at a dose of about 5.2×10^7 Gy. They used white-beam exposure of the crystal and the correlation coefficient between structure factors extracted from Laue images to assess the damage. The small difference may arise from the different way that the radiation damage was assessed as well as uncertainties in the dose estimation in their study.

The positive electron-density peaks observed in the difference map were less significant than the negative ones. Most of them are in proximity to negative electron-density peaks and arise from movements of side chains or to a relaxation of the main chain when a neighbouring group is lost or when a disulfide bridge is cleaved. There is some evidence for changes in the solvent structure and changes of the relative occupancies for side-chain rotamers in serine and threonine.

There is no evidence for preferred reactions which form adducts as might be expected, for example, from attack by hydroxyl radicals. However, from a crystallographic study, a background of adduct formation leading to low occupancies cannot be excluded; in particular, nothing can be said about protonation reactions which are observed by electron-spin resonance (Liming & Gordy, 1968; Sevilla *et al.*, 1979). There may be a significant background of chemical modifications which contribute to the reduction of diffraction from a protein crystal during radiation damage but which are not evident in the electron density. Strand breakage (Liming & Gordy, 1968) also cannot be excluded.

Another hypothesis for the reduction in diffraction would be a loss of specific interactions at the crystal contacts (for example, if carboxylic acid residues involved in intermolecular salt bridges are lost). This may lead to slow movements of the protein molecule despite the frozen state of the solvent, especially as the solvent undergoes structural changes owing to the accumulation of radicals. However, in the case of myrosinase no labile residues are involved in crystal contacts.

Despite the frozen state of the protein at 100 K, significant movements of the protein chain still seem to be possible which are induced either by the loss of salt bridges or disulfide bonds.

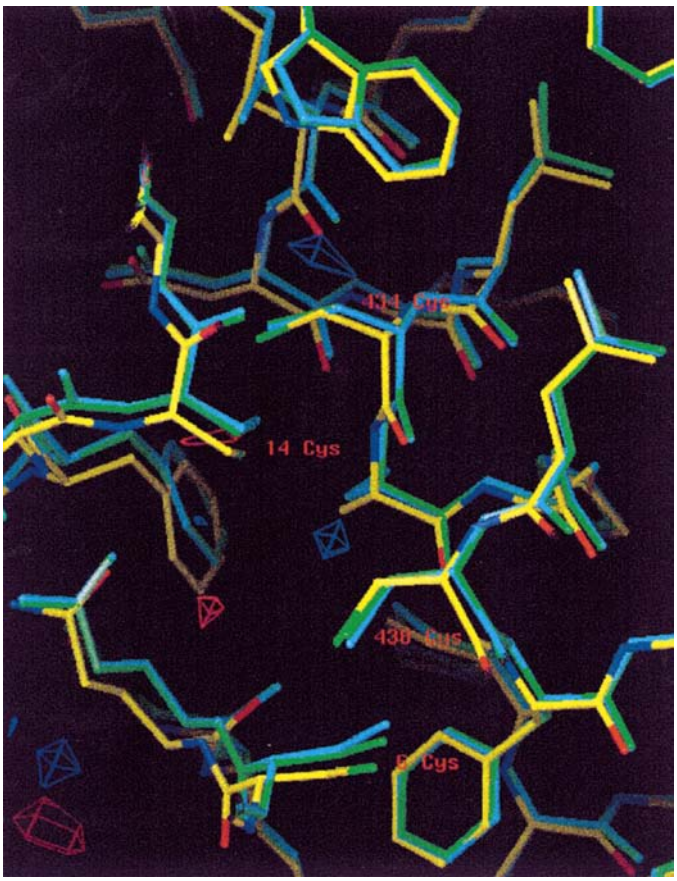

Figure 6
Comparison of the structure in the vicinity of the disulfide bridges Cys14–Cys434 and Cys6–Cys438 before and after breakage of the disulfide bridges owing to radiation damage. The structure which was refined to 2.4 Å resolution against data set 4 collected after irradiation with a dose of 54×10^{15} photons mm^{-2} is shown in yellow, together with a structure (cyan) refined in the same way against data set 0 collected prior to irradiation and the 1.2 Å reference structure (green). The electron density of a $F_{obs} - F_{calc}$ map calculated after refinement of the structure of the irradiated protein contoured at $\pm 3\sigma$ is shown in blue and red. The highest positive electron densities correspond to alternate rotamer positions of S^{γ}.

4.2. Disulfide bridges

The susceptibility of disulfide bridges to radiation damage is in agreement with the ease of radical formation of disulfide bridges. The damage may be initiated either by trapping of electrons (1*a*), holes (1*d*) or radical attack (1*e*) (Fig. 1). Subsequently, the disulfide bridge may be cleaved either without the action of additional radicals or molecules (1*b*) or under the action of water molecules (1*e*) or hydroxyl anions (1*f*). A direct cleavage by radical attack (1*e*) is also possible. Because all the disulfide bridges in this protein are partially exposed to the solvent, it is not possible to exclude some reaction mechanisms. Reactions such as those shown in (2*a*) and (2*b*) leading to a cleavage of the carbon–sulphur bond are probably observed in these experiments as the occupancy of the S atoms in the open disulfide bridges is smaller than 1.0, although it cannot be ruled out that this is caused by a disorder of the S atom involving the presence of several rotamers. In this study, the formation of sulfonyl groups (*R*SOH) at the cysteines can be neither confirmed nor ruled out, as the group may be disordered or as its occupancy may be too low. In the structure of rat neonatal Fc receptor, where the breakage of disulfide bridges was first described (Burmeister *et al.*, 1994), only one of the three disulfide bonds is accessible to solvent. The disulfide-bridge breakage was only observed for this group, which suggests that the breakage may not occur so easily for buried disulfide bridges.

For one of the free cysteine residues (Cys73) a loss of occupancy of the S atom is observed, indicating cleavage of the carbon–sulfur bond. Possible mechanisms for this cleavage are given in (2*a*) and (2*b*). This may be because of the solvent exposure of the S atom, which is buried in the other residue; however, more observations will be needed for a definitive answer.

4.3. Carboxylic acids

In the literature, decarboxylation has mainly been observed for the main-chain carboxyl groups of short peptides and for carboxylic acids. The suggested mechanism is the transfer of an electron hole to the carboxyl group, which leads to the formation of CO_2 and a carbon-centred radical (Box *et al.*, 1969, 1972; Sevilla *et al.*, 1979). The corresponding reaction is shown in (3*a*) and (3*b*) of Fig. 1. Sevilla & D'Arcy (1977) describe an enhancement of the decarboxylation reaction owing to the proximity of a photoionizable aromatic group. The possibility of a direct electron transfer may be an explanation of why hydrogen-bonded pairs of tyrosine and glutamic acid residues seem to be particularly reactive.

The protection of the carboxyl groups coordinating the structural Zn atom is very pronounced. Owing to its positive charge, the Zn atom may trap free electrons, leading to lower oxidation states such as Zn^{+} *etc*. The trapped electron could be transferred rapidly to holes which were formed on the coordinating carboxyl groups as shown in (3*a*), protecting these groups efficiently from decarboxylation.

4.4. Tyrosine

The only reactions described for tyrosine residues are shown in Fig. 1. After the loss of an electron (or the capture of a hole) a positively charged tyrosine radical is formed (4*a*), which deprotonates to form a phenoxyl radical (4*b*). This radical is supposed to be quite stable and so far there is no explanation of how the observed loss of the hydroxyl group occurs. Since the most labile hydroxyl groups are hydrogen bonded to carboxylic acid, this suggests the possible assistance of a carboxyl group or the radical which has been formed after decarboxylation. It cannot be completely ruled out that the apparent loss of electron density for the hydroxyl group is because of a hinge-like motion of the tyrosine ring around C^{β} in the absence of stabilization by the hydrogen bond to the glutamic acid residue. Such an increase of disorder or thermal agitation would be most prominent for the hydroxyl group.

4.5. Methionine

Methionine residues have not been well studied so far in terms of possible reaction mechanisms. A preferential formation of sulfur-centred radicals was described (Shields & Gordy, 1958), but without a more detailed characterization of the radical or its reaction products. According to Shimazu *et al.* (1964), a cleavage according to reaction (5) is likely. Interestingly, the most labile groups are fully buried inside the hydrophobic core of the protein, excluding the involvement of the solvent in the reaction.

4.6. Outlook

The question arises as to whether protection against radiation damage can be achieved using suitable additives. A promising method may be the use of *t*-butanol, which is a good scavenger for hydroxyl radicals in the liquid state (Rao & Hayon, 1974). The contribution of hydroxyl radicals to the radiation-damage process at low temperatures is still to be established. Furthermore, the mobility of hydroxyl radicals at low temperature must be high enough for the protectant to be efficient. Another target would be the inclusion of Fe^{3+}-containing compounds such as $FeCN_6^{3-}$ (Jones *et al.*, 1987) which may act as an acceptor for mobile electrons. The electron may be preferentially transferred to a Fe atom which could be reduced, preventing electron transfer to disulfide bridges, where a cleavage of the bridge may follow. On the other hand, there is a trade-off between protective effects and increased radiation damage arising from increased absorption in the sample. The stability of protein crystals in the presence of such compounds also has to be considered.

The question of the dose-rate dependence of the radiation damage will have to be assessed. It is possible to think of dose-rate-dependent mechanisms. At a higher dose rate the concentration of radicals and free electrons will be higher and more recombination events may occur. For example, the electron holes, which are located particularly on carboxylic acid groups or disulfide bridges, may recombine with free electrons before they lead to decarboxylation. The consequence would be less radiation damage at higher fluxes. On

the other hand, if double-excitation events play a role in radiation-damage mechanisms, then the damage would be more important at a higher dose rate. Future experiments at variable dose rates are needed in order to answer this question.

5. Implications for synchrotron data collection

5.1. Instrumentation

Until now, the atomic structure of a protein determined by X-ray crystallography has been considered to be insensitive to radiation damage. Radiation damage has only been noticed as a global effect in the form of a reduction of the diffracted intensity from a protein crystal. The possibility of introducing artefacts owing to the X-ray irradiation of cryo-cooled crystals necessitates careful thought about the X-ray doses a protein crystal receives. It is obvious that synchrotron beamlines should provide exact information on the X-ray dose used in a data collection. This information would best be specified in photons mm^{-2}. The dose deposited in the sample (measured in Gray) depends on its elemental composition and thus cannot be given by the beamline instrumentation. For a weakly absorbing sample, the dose can be easily calculated based on the elemental composition, its density and the energy of the X-rays. It would be even more convenient if data collections were to be carried out in dose mode; this means exposing each image to a given dose (photons mm^{-2}) and not for a certain period of time. Experiments carried out at different experimental stations or during different modes of operation of a synchrotron could be directly compared.

Radiation doses should be kept as low as possible. In order to achieve this, the best signal-to-noise ratio is needed, which implies the use of detectors with the best detective quantum efficiency (DQE). Furthermore, all sources of diffuse scatter should be minimized, which means an adjustable beam size so that it can be matched to the size of the crystal, a short path of the X-ray beam in air and as little material as possible around the crystal (small drops of cryoprotectant).

5.2. Strategy of data collections

The first practical aspect is to collect low-resolution data sets before high-resolution data sets in cases where the high-resolution data set contains too many overloaded reflections at lower resolution. The contribution of the low-resolution data set to the total structure is quite important, as the total intensity in the reflections at lower resolution is higher than the total intensity in the high-resolution reflections, which is a consequence of the rapid decrease of intensity with resolution caused by the temperature factor and the atomic form factor. On the other hand, the X-ray dose needed for the collection of the low-resolution data set can be neglected compared with the dose needed for the high-resolution pass. If the low-resolution data set is collected first, it corresponds to the native structure. If the low-resolution data set is collected after the high-resolution data set, it may correspond to a state with heavy radiation damage. This is the current practice followed by most synchrotron users.

The use of a strategy option (in *MOSFLM*) or a strategy program (Ravelli *et al.*, 1997, for *DENZO*) is advisable in order to obtain a complete data set with the minimum radiation dose. Collecting more data may lead to better data sets owing to the higher redundancy, but if the radiation dose is not monitored it may just lead to a degradation of the data quality owing to the contribution of a structure showing heavy radiation damage (linked to an increase in $R_{\rm merge}$).

In general, it is still advisable to try to obtain crystals of a reasonable size in order to keep the radiation dose small. Data sets which are collected on very small crystals showing extensive decay during the data collection are unlikely to lead to very high quality structures and often show relatively high crystallographic R factors. From day-to-day experience, the crucial limit is situated somewhere below $30 \times 30 \times 30$ µm, obviously depending on the unit-cell size, space group, solvent content and the internal order of the crystal.

One way of monitoring the extent of radiation damage would be to collect the first few frames of a data set again at the end of the data collection. The increase in the temperature factor or the reduction in the diffracted intensity for the same X-ray dose in the exposure should give an indication of the extent of radiation damage. It may also be possible to use the increase of the unit-cell volume as a measure of the absorbed dose.

5.3. Design of experiments

Radiation effects become very important in experiments where different redox states of the same protein are to be observed. The experiment has to be designed such that the desired state is still present at the end of the data collection. It should be kept in mind that metal centres are preferred sites for reduction as electrons will be transferred easily (Jones *et al.*, 1987).

If subtle ligand-induced changes are to be observed, monitoring of the X-ray dose is essential in order to make sure that differences are not caused by radiation damage. In order to obtain meaningful results, only data sets collected with the same total dose should be compared; otherwise, differences could merely be a consequence of the different radiation dose.

In a multiple anomalous dispersion (MAD) experiment, where very accurate measurements of intensities are essential, the radiation dose should be controlled in order to minimize the introduction of non-isomorphism. In the case of MAD experiments on selenomethionine-substituted proteins, the problem can be even more serious if the analogous reaction to the loss of the methylthio group in methionine also occurs for selenomethionine. From the point of view of radiation damage, it is best to change the energy after the collection of a small segment of data. The same reflection would be collected several times at different wavelengths after a similar radiation dose had been absorbed in the crystal. A difference in intensity would only arise from changes in f' and f'' and not from radiation-induced changes of the structure. Radiation damage

which occurs slowly over the duration of the experiment can be taken into account by treating the data in several batches. There may be slight changes of the structure or of Se-atom occupancies from batch to batch, which can be handled by the software used for phasing.

With the third generation of synchrotron sources, the intrinsic limit of information which can be extracted from a given crystal has been reached. This means there is a limitation in either the minimum size of the crystal which can be used for a full data set or in the highest resolution of diffraction data which can be obtained from a given crystal. Further progress should still be possible with the development of protective agents, the use of multiple crystals and the increase of the instrumental precision of experiments in order to obtain more information from a crystal for a given radiation dose.

I would like to thank Carl-Ivar Brändèn, Stephen Cusack, Elspeth Garman and Raimond Ravelli for discussions and references to the literature. I am grateful to Steffi Arzt and Soichi Wakatsuki for the critical reading of the manuscript and to Sandro Palmieri for the supply of the protein.

References

Berthet-Colominas, C., Monaco, S., Novelli, A., Sibaï, G., Mallet, F. & Cusack, S. (1999). *EMBO J.* **18**, 1124–1136.
Bonifacic, M. & Asmus, K.-D. (1976). *J. Phys. Chem.* **80**, 2426–2430.
Bonifacic, M., Schäfer, K., Möckel, H. & Asmus, K.-D. (1975). *J. Phys. Chem.* **79**, 1496–1502.
Box, H. C., Budzinski, E. E. & Lilga, K. T. (1972). *J. Chem. Phys.* **57**, 4295–4298.
Box, H. C., Freund, H. G., Lilga, K. T. & Budzinski, E. E. (1969). *J. Phys. Chem.* **74**, 40–52.
Brünger, A. T. (1992*a*). *X-PLOR Version* 3.1. *A System for Crystallography and NMR.* Yale University, New Haven, Connecticut, USA.
Brünger, A. T. (1992*b*). *Nature (London)*, **355**, 472–475.
Burmeister, W. P., Bourgeois, D., Kahn, R., Belrhali, H., Mitchell, E. P., McSweeney, S. M. & Wakatsuki, S. (1998). *Proc. Soc. Photo-Opt. Instrum. Eng.* **3448**, 188–196.
Burmeister, W. P., Cottaz, S., Driguez, H., Iori, R., Palmieri, S. & Henrissat, B. (1997). *Structure*, **5**, 663–675.
Burmeister, W. P., Cottaz, S., Driguez, H., Rollin, P., Vasella, A. & Henrissat, B. (2000). In the press.
Burmeister, W. P., Gastinel, L. N., Simister, N. E., Blum, M. L. & Bjorkman, P. J. (1994). *Nature (London)*, **372**, 336–343.
Collaborative Computational Project, Number 4 (1994). *Acta Cryst.* D**50**, 760–763.
Dejus, R. J. & Sánchez del Río, M. (1996). *Rev. Sci. Instrum.* **67**(9), 3356.
Gonzalez, A. & Nave, C. (1994). *Acta Cryst.* D**50**, 874–877.
Gonzalez, A., Thompson, A. & Nave, C. (1992). *Rev. Sci. Instrum.* **63**, 1177–1180.
Henderson, R. (1990). *Proc. R. Soc. London Ser. B*, **241**, 6–8.
Hope, H. A. (1988). *Acta Cryst.* B**44**, 22–26.
Jones, G. D. D., Lea, J. S., Symons, M. C. R. & Taiwo, F. A. (1987). *Nature (London)*, **330**, 772–773.
Jones, T. A., Bergdoll, M. & Kjeldgaard, M. (1993). *Crystallographic Computing and Modeling Methods in Molecular Design*. New York: Springer.
Leslie, A. G. W. (1990). *Crystallographic Computing.* Oxford University Press.
Liming, F. G. Jr & Gordy, W. (1968). *Proc. Natl Acad. Sci. USA*, **60**, 794–801.
Murshudov, G. N., Lebedev, A., Vagin, A. A., Wilson, K. S. & Dodson, E. J. (1999). *Acta Cryst.* D**55**, 247–255.
Rabus, H., Scholze, F., Thornagel, R. & Ulm, G. (1996). *Nucl. Instrum. Methods A*, **377**, 209–216.
Rao, D. N. R., Symons, M. C. R. & Stephenson, J. M. (1983). *J. Chem. Soc. Perkin Trans.*, pp. 727–730.
Rao, P. S. & Hayon, E. (1974). *J. Phys. Chem.* **78**, 1193–1196.
Ravelli, R. B. G. & McSweeney, S. M. (2000). In the press.
Ravelli, R. B. G., Sweet, R. M., Skinner, J. M., Duisenberg, A. J. M. & Kroon, J. (1997). *J. Appl. Cryst.* **30**, 551–554.
Sevilla, M. D. & D'Arcy, J. B. (1977). *J. Phys. Chem.* **82**, 338–342.
Sevilla, M. D., D'Arcy, J. B. & Morehouse, K. M. (1979). *J. Phys. Chem.* **83**, 2887–2892.
Shields, H. & Gordy, W. (1958). *J. Phys. Chem.* **62**, 789–798.
Shimazu, F., Kumta, U. S. & Tappel, A. L. (1964). *Radiat. Res.* **22**, 276–287.
Sonntag, C. von (1987). *The Chemical Basis of Radiation Biology.* London: Taylor & Francis.
Sonntag, C. von & Schuchmann, H.-P. (1994). *Methods Enzymol.* **233**, 3–21.
Weik, M., Ravelli, R. B. G., Kryger, G., McSweeney, S. M., Raves, M. L., Harel, M., Gros, P., Silman, I., Kroon, J. & Sussman, J. L. (2000). *Proc. Natl Acad. Sci. USA*, **97**(2), 623–628.